Available online at www.sciencedirect.com
SCIENCE DIRECT
ELSEVIER
Journal of the European Ceramic Society 26 (2006) 2827–2832
ECERS
www.elsevier.com/locate/jeurceramsoc

Crystal structure, thermal expansion and electrical conductivity of perovskite oxides $Ba_xSr_{1-x}Co_{0.8}Fe_{0.2}O_{3-\delta}$ ($0.3 \leq x \leq 0.7$)

Bo Wei [a,b], Zhe Lü [a,b], Xiqiang Huang [a,b], Jipeng Miao [a,b], Xueqing Sha [a,b], Xianshuang Xin [a,b], Wenhui Su [a,b,c,d,*]

[a] *Center for Condensed Matter Science and Technology, Harbin Institute of Technology, Harbin 150001, PR China*
[b] *Key Laboratory of the Condensed-Matter Science and Technology, Harbin Institute of Technology, HeiLongJiang Provincial Universities, Harbin 150001, PR China*
[c] *Department of Physics, Jilin University, Changchun 130023, PR China*
[d] *International Center for Materials Physics, Academia Sinica, Shenyang 110015, PR China*

Received 10 March 2005; received in revised form 16 June 2005; accepted 26 June 2005
Available online 22 August 2005

Abstract

$Ba_xSr_{1-x}Co_{0.8}Fe_{0.2}O_{3-\delta}$ ($0.3 \leq x \leq 0.7$) composite oxides were prepared and characterized. The crystal structure, thermal expansion and electrical conductivity were studied by X-ray diffraction, dilatometer and four-point DC, respectively. For $x \leq 0.6$ compositions, cubic perovskite structure was obtained and the lattice constant increased with increasing Ba content. Large amount of lattice oxygen was lost below 550 °C, which had significant effects on thermal and electrical properties. All the dilatometric curves had an inflection at about 350–500 °C, and thermal expansion coefficients were very high between 50 and 1000 °C with the value larger than $20 \times 10^{-6}\,°C^{-1}$. The conductivity were larger than $30\,S\,cm^{-1}$ above 500 °C except for $x > 0.5$ compositions. Furthermore, conductivity relaxation behaviors were also investigated at temperature 400–550 °C. Generally, $Ba_{0.4}Sr_{0.6}Co_{0.8}Fe_{0.2}O_{3-\delta}$ and $Ba_{0.5}Sr_{0.5}Co_{0.8}Fe_{0.2}O_{3-\delta}$ are potential cathode materials.

Keywords: Perovskites; SOFC cathodes; Thermal expansion; Electrical conductivity; (Ba,Sr) $(Co,Fe)O_3$

1. Introduction

In the past decades, there has been growing interest in perovskite-type oxides with mixed oxygen-ionic and electronic conductivity (MIEC), which are attractive materials for solid oxide fuel cell (SOFC) cathodes, oxygen separation membranes and other applications.[1–5] For example, compositions of $(La,Sr)(Co,Fe)O_{3-\delta}$ were extensively investigated. With partial substitution of La^{3+} by Sr^{2+} in A-site, oxygen vacancies as well as valence changes of B-site ions occur in order to maintain the electrical neutrality, which is the reason for ionic and electronic conductivity. Although the ionic conductivity in these materials usually accounts for less than 1% of the overall electrical conductivity, it remains 1–2 orders of magnitude higher than that found for yttria stabilized zirconia (YSZ).[3]

About 20 years ago, Teraoka et al. first reported $SrCo_{0.8}Fe_{0.2}O_{3-\delta}$ (SCF) membranes with very high oxygen permeation flux, which is attributed to the high concentration of oxygen vacancy, caused by the substitution of A^{3+} metal ion by Sr^{2+} in the A-site of perovskite.[6] Huang et al. have studied the properties of SCF as a cathode material for SOFC.[7] Unfortunately, a perovskite–brommillerite transition could occur at lower oxygen partial pressure (<0.1 atm) and at lower temperatures, making the membrane fractured.[8] With the purpose of improving the phase stability and keeping the high performance, Shao et al. developed $Ba_xSr_{1-x}Co_{0.8}Fe_{0.2}O_{3-\delta}$ ($x > 0$, BSCF) perovskite series by a proper substitution of strontium in SFC. Their permeation behaviors, phase stability, mechanical strength, etc. have been extensively investigated, especially for the

* Corresponding author. Tel.: +86 451 8641 8440; fax: +86 451 8641 2828.
E-mail address: suwenhui@hit.edu.cn (W. Su).

0955-2219/$ – see front matter © 2005 Elsevier Ltd. All rights reserved.
doi:10.1016/j.jeurceramsoc.2005.06.047

$Ba_{0.5}Sr_{0.5}Co_{0.8}Fe_{0.2}O_{3-\delta}$ composition.[9–11] Recently, Shao et al. also presented $Ba_{0.5}Sr_{0.5}Co_{0.8}Fe_{0.2}O_{3-\delta}$ as a novel cathode material for the next generation of SOFCs.[12] With thin-film samarium doped ceria (SDC) as electrolyte, single cells exhibited considerable high densities at lower temperatures (1010 and 402 mW cm^{-2} at 600 and 500 °C, respectively).

So far, only $Ba_{0.5}Sr_{0.5}Co_{0.8}Fe_{0.2}O_{3-\delta}$ composition has been studied for SOFC cathode,[12] other compositions in the BSCF system have not been reported. From the viewpoint of SOFC applications, except for good electrochemical performances, a satisfactory cathode material must also meet other requirements such as thermal expansion match with other components. Besides, the electrical conductivity, another basic parameter of cathode materials, also needs to be investigated. In the present study, oxides with fixed B-site ratio in the system of $Ba_xSr_{1-x}Co_{0.8}Fe_{0.2}O_{3-\delta}$ ($0.3 \le x \le 0.7$) were prepared and characterized. The effects of Ba content on the crystalline structure, thermal expansion behaviors and electrical conductivities were examined in order to determine the suitability of BSCF as SOFC cathode materials.

2. Experimental

2.1. Sample preparation

Composite oxides of the $Ba_xSr_{1-x}Co_{0.8}Fe_{0.2}O_{3-\delta}$ ($0.3 \le x \le 0.7$) compounds were synthesized via a modified sol–gel method, using ethylenediamine tetraacetic acid (EDTA) and citric acid as complexes.[4] The starting reagents used were $Ba(NO_3)_2$, $Sr(NO_3)_2$, $Co(NO_3)_2{\cdot}6H_2O$, $Fe(NO_3)_3{\cdot}9H_2O$, EDTA and citric acid, all of which were reagent grade (>99%). The precursors obtained were calcined at 950 °C for 5 h in air to get the single-phase compositions. These powers were then pressed into green disks at about 300 MPa followed by sintering at 1100–1150 °C in stagnant air for about 5–6 h to get dense samples.

2.2. Characteristics measurements

The crystal structure of each BSCF composition was examined by X-ray powder diffraction (XRD, Bede D^1 X-ray Diffractometer) using Cu Kα radiation. Thermal expansion coefficients (TECs) were measured by a dilatometer (Netzsch DIL 402C/3/G) in the temperature range 50–1000 °C in air with the heating rate of 2 °C min^{-1}. Both electrical conductivity and conductivity relaxation were measured in air by the four-point DC method using a digital Sourcemeter (Keithley 2400) and a programmed-temperature controller (Yuguang AI 808P). The measurements were for conductivity was carried out from room temperature to 900 °C, while conductivity relaxation for $x = 0.4$ sample was measured at temperature 400–550 °C.

3. Results and discussion

3.1. Crystal structure

The XRD patterns of the $Ba_xSr_{1-x}Co_{0.8}Fe_{0.2}O_{3-\delta}$ ($0.3 \le x \le 0.7$) oxides measured at room temperature are illustrated in Fig. 1. As can be seen, for $0.3 \le x \le 0.6$ compositions, pure phases are formed which can be indexed as cubic perovskite structure with a space group of *Pm*-3*m* (2 2 1),[9] indicating that the tolerance factor for these perovskites is around 1. For $x = 0.7$, namely $Ba_{0.7}Sr_{0.3}Co_{0.8}Fe_{0.2}O_{3-\delta}$, the XRD pattern can be basically considered as perovskite structure with slight additional peaks.

From the XRD patterns, it can also be seen that the main peak around $2\theta = 32°$ shifts gradually left to lower degrees from $x = 0.3$ to 0.7, indicating that the lattice parameter increases with doping content of barium, which agrees with the calculated results given below. The lattice parameters and unit cell volumes are plotted in Fig. 2. The lattice parameter of SCF ($a = 0.38630$ nm[4]) is also given for comparison. It is obvious that both of them increase constantly with increasing Ba content. The dimension expands about 7.1% from $x = 0.3$ to 0.7. As both Sr and Ba in A-site are bivalent, it can be

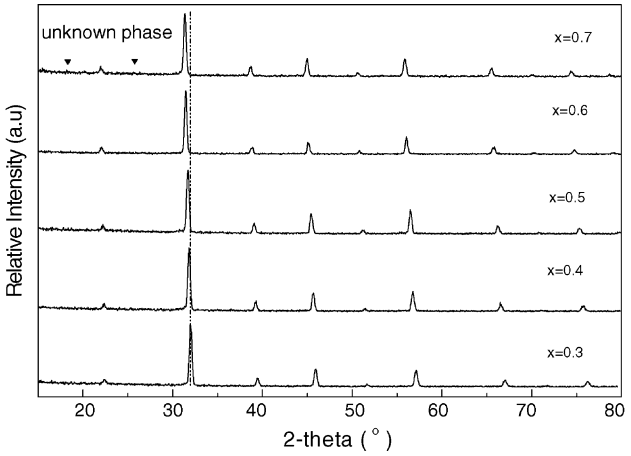

Fig. 1. XRD patterns of $Ba_xSr_{1-x}Co_{0.8}Fe_{0.2}O_{3-\delta}$ oxides.

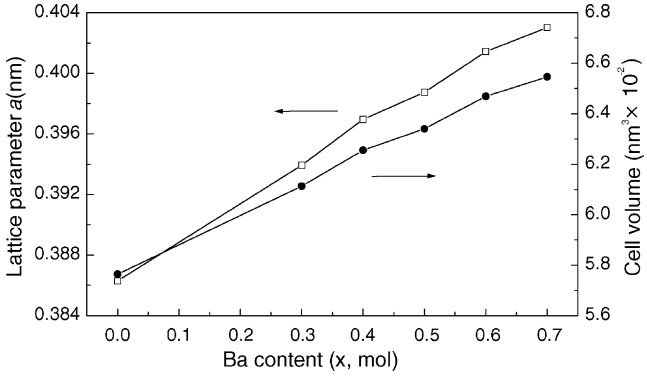

Fig. 2. Lattice parameter and cell volume as a function of Ba content in $Ba_xSr_{1-x}Co_{0.8}Fe_{0.2}O_{3-\delta}$.

Table 1
Ionic radii for several cations in the perovskite lattices

Cation	Ionic radius (nm)
Ba^{2+}	0.175 (CN[a] = 12)
Sr^{2+}	0.158 (CN = 12)
Co^{2+}	0.0885 (CN = 6) HS[b]
Co^{3+}	0.075 (CN = 6) HS
Co^{4+}	0.067 (CN = 6) HS
Fe^{3+}	0.0785 (CN = 6) HS
Fe^{4+}	0.0725 (CN = 6)

[a] CN, coordination number.
[b] HS, high spin.

assumed that the introduction of barium has slight effect on the valence states of Co and Fe. Therefore, the changes can be primarily attributed to the fact that the radius of Ba^{2+} is larger than that of Sr^{2+}. In Table 1, the ionic radii of cations involved in this paper are given, according to Shannon.[13]

3.2. Thermal expansion

Thermal expansion data obtained upon heating for BSCF compositions, as well as their first derivative (namely, thermal expansion coefficients), are given in Figs. 3 and 4,

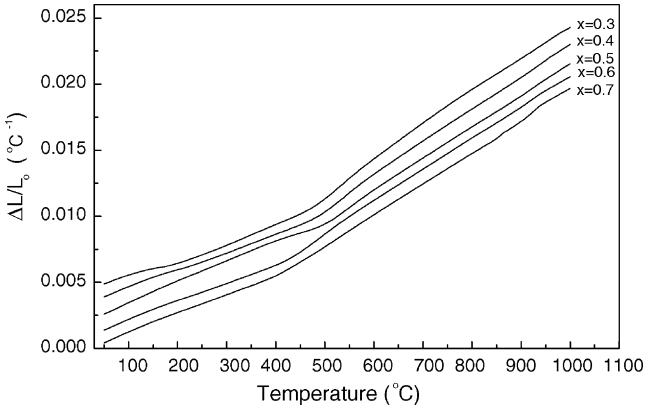

Fig. 3. Thermal expansion curves for $Ba_xSr_{1-x}Co_{0.8}Fe_{0.2}O_{3-\delta}$.

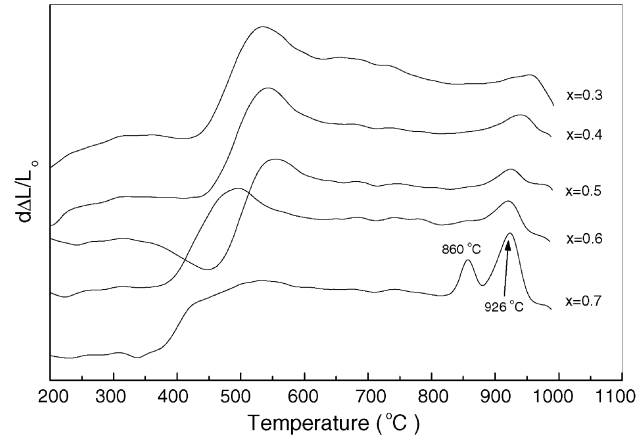

Fig. 4. First derivative of $\Delta L/L_o$ vs. temperature for $Ba_xSr_{1-x}Co_{0.8}Fe_{0.2}O_{3-\delta}$.

respectively. As can be seen in Fig. 3, the thermal expansion behavior in this system is relatively abnormal, all of which are nonlinear with inflection occurring between about 350 and 550 °C. Basically, $\Delta L/L_o$ increases upon heating at the beginning stage, then begin to experience a curving range and flatten again at elevated temperatures. The appearance of these inflection points, occurring at such moderate temperature ranges, can mainly be attributed to the loss of lattice oxygen (so-called β-desorption of oxygen[14]) and the formation of oxygen vacancies. Simultaneously, the reduction of the Fe and Co ions must occur in order to maintain the electrical neutrality.[15–17] Related thermal reductions of cations in B-site, from high valence state of Co^{4+} and Fe^{4+} to lower trivalent of Co^{3+} and Fe^{3+}, are described in Eqs. (1) and (2), respectively.[9,15] These can be described according to the defect reaction (in the Kröger–Vink notation).

$$2Co_{Co}^{\bullet} + O_o^{\times} \Leftrightarrow 2Co_{Co}^{\times} + V_o^{\bullet\bullet} + \tfrac{1}{2}O_2 \quad (1)$$

$$2Fe_{Fe}^{\bullet} + O_o^{\times} \Leftrightarrow 2Fe_{Fe}^{\times} + V_o^{\bullet\bullet} + \tfrac{1}{2}O_2 \quad (2)$$

The valence changes are also associated with an increase of the ionic radius, as can be seen in Table 1, especially for the reduction of Co^{4+} to Co^{3+}. Accordingly, the reductions cause a decrease in the B–O bond according to Pauling's second rule, and hence the size of BO_6 octahedra increases, thus enhancing the lattice expansion.[16] Correspondingly, the TEC results exhibit obvious changes in Fig. 4 at the same temperature range. In addition, it also can be seen in Fig. 4 that the $d\Delta L/L_o$ curves show another one or two peaks around 900 °C, where the TEC change stair(s) occur. It is reported that tri-valent state Co^{3+} can be further reduced to Co^{2+} in this temperature range, accomplished by the further desorption of lattice oxygen.[9]

$$2Co_{Co}^{\times} + O_o^{\times} \Leftrightarrow 2Co_{Co}^{'} + V_o^{\bullet\bullet} + \tfrac{1}{2}O_2 \quad (3)$$

The characteristic temperature for the thermal reduction of Fe^{3+} to lower Fe^{2+} in air, on the other hand, is reported to be 1560 °C.[14] The abnormal behavior of the $x = 0.7$ compound may be attributed to the unknown phase or possible phase transition. The large radius change from Co^{3+} to Co^{2+} should take place. But no obvious increase in TEC value is observed, which is the subject for further research. High temperature XRD may be effective to clarify the phenomena. Note that high concentration of oxygen vacancies have reached, which may show negative contribution on lattice expansion. Generally, in the system of (La,Sr)(Co,Fe)$O_{3-\delta}$, their thermal expansion curves are relative linear below 800 °C and exhibit abnormal expansion at high temperatures due to reduction in oxygen content.[15] On the contrary, in these BSCF compositions, high concentration of oxygen vacancy in lattice can be achieved at lower temperature, which can result in the curving region shifts to lower temperatures. From this point of view, the structure of BSCF may be relative unstable, compared with LSCF. But it has positive effects on the cathode performance.

Table 2
Specific TEC values for $Ba_xSr_{1-x}Co_{0.8}Fe_{0.2}O_{3-\delta}$

$Ba_xSr_{1-x}Co_{0.8}Fe_{0.2}O_{3-\delta}$	TEC ($10^{-6}\,^{\circ}C^{-1}$)		
	50–1000 °C	500–700 °C	500–1000 °C
$x=0.3$	20.44	28.74	25.98
$x=0.4$	20.12	26.87	25.38
$x=0.5$	19.95	24.95	24.26
$x=0.6$	20.18	24.57	23.80
$x=0.7$	20.27	23.79	23.98

It is well-known that the Co-based perovskites generally have quite high TECs, which are often about $20\times10^{-6}\,^{\circ}C^{-1}$,[18] such as the TEC of $La_{0.3}Sr_{0.7}Co_{0.8}Fe_{0.2}O_{3-\delta}$ is about $21.0\times10^{-6}\,^{\circ}C^{-1}$ (30–1000 °C).[19] Average thermal expansion coefficients for BSCF series calculated are listed in Table 2. As can be seen, all of the TEC values are larger than $20\times10^{-6}\,^{\circ}C^{-1}$ in the whole measured range. Especially, the TEC values between 500 and 700 °C, the range at which the intermediate-temperature SOFCs perform, are also listed. Note that their TEC values between 500 and 700 °C are extraordinarily high and decrease from $28.74\times10^{-6}\,^{\circ}C^{-1}$ ($x=0.3$) to $23.79\times10^{-6}\,^{\circ}C^{-1}$ ($x=0.7$). While, the decreasing rate inclines to be slower. Even the minimum is still nearly twice than that of solid electrolytes used for IT-SOFCs (e.g. TEC_{SDC} is about $12\times10^{-6}\,^{\circ}C^{-1}$). Accordingly, the issue of thermal matching between the cathode and electrolyte should take into account carefully for SOFC applications.

3.3. Electrical conductivity

Generally, there are two kinds of conductive mechanisms (namely, electronic and ionic conductivity) in these perovskite oxides, owing to the co-presence of holes and oxygen vacancies. While, the ionic conductivity is much lower than the electronic conductivity. Therefore, it can be assumed reasonably that the measured values refer to the electronic conductivity alone.[20]

The logarithm of electrical conductivity versus reciprocal temperature of different BSCF compositions is shown in Fig. 5. As can be seen, the electrical conductivity of all compounds increases gradually with temperature up to about 400–500 °C. As discussed above, the lattice oxygen becomes more active at this temperature range. Along with the thermal induced lattice oxygen losses, more oxygen deficiency is formed, which thus causes the thermal reduction of Co and Fe cations to lower states, described in Eqs. (1) and (2). Note that their electrical characteristics are not similar at elevated temperatures. The electrical conductivity of $x=0.3$ reaches a maximum of 59.2 S cm^{-1} at about 539 °C and then decreases continuously. While, for $x=0.4$ and 0.5, it decreases slightly from about 540 to 570 °C and then turns to increase again slightly from about 800 °C. When $x=0.6$ and 0.7, however, it continues increasing with elevated temperature. As given in Eq. (3), Co^{3+} will be further reduced to lower oxidation

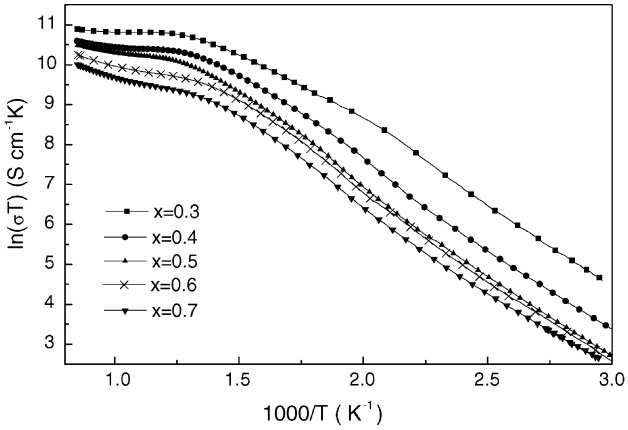

Fig. 5. $\ln \sigma T$ vs. $1000/T$ in air for $Ba_xSr_{1-x}Co_{0.8}Fe_{0.2}O_{3-\delta}$.

state Co^{2+}, which further affects the electrical property. Here, as can be seen, the expansion and the conductivity results agree with each other. Furthermore, the results are also consistent with the O_2-TPD results for these BSCF compositions ($x=0.3$, 0.5 and 0.7), which exhibited oxygen desorption peaks at similar temperature ranges. The thermal reduction for transition metals tends to be easier with the increase of Ba doping.[9] These may explain the reason for the different behaviors at higher temperature zone. Besides, oxygen vacancy order also may show contribution to the observed phenomena.

Specific conductivities of each BSCF compound at various temperatures are shown in Fig. 6. It can be observed that the electrical conductivity decreases with the increasing doping of barium, in the whole measured temperature range. When $x\leq0.5$, the values are typically larger than 30 S cm^{-1}. Although the conductivity values measured are lower than that of other cathode materials, they are still acceptable for cathode applications. The continuous loss of lattice oxygen upon heating can lead to the increase of oxygen vacancies concentration, which thus can enhance the oxide ionic conductivity. High ionic conductivity can be obtained at lower temperature, which is the important reason for $Ba_{0.5}Sr_{0.5}Co_{0.8}Fe_{0.2}O_{3-\delta}$ to exhibit remark-

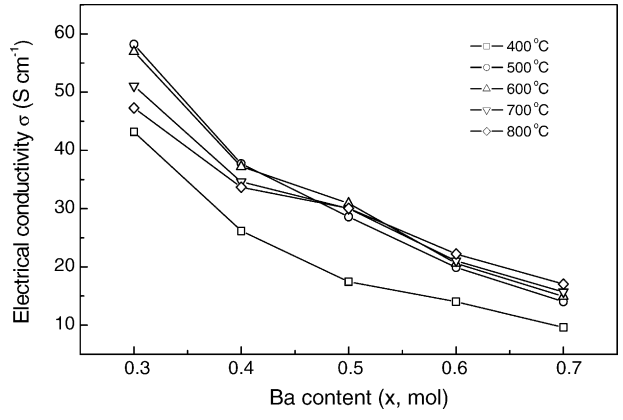

Fig. 6. Specific conductivity values at various temperature points.

Table 3
Activation energy E_a for the electrical conductivity of $Ba_xSr_{1-x}Co_{0.8}Fe_{0.2}O_{3-\delta}$

$Ba_xSr_{1-x}Co_{0.8}Fe_{0.2}O_{3-\delta}$	Temperature range (°C)	E_a (kJ mol^{-1})
$x=0.3$	100–430	31.2
$x=0.4$	100–450	36.6
$x=0.5$	100–450	38.6
$x=0.6$	100–420	38.3
$x=0.7$	100–450	37.1

able electrochemical performance, compared with LSCF or $Sm_{0.5}Sr_{0.5}CoO_{3-\delta}$ (SSC) at 500–600 °C.

As proved by thermopower method, the conductivity mechanism for BSCF series can be attributed to the hopping of P-type small polarons.[21] The localized electronic charge carriers have a thermally activated mobility. If the carrier concentration remains constant throughout the temperature range measured, the Arrhenius plot for small polaron conduction should be linear ($\ln \sigma T$ versus $1000/T$), following the formula relation:

$$\sigma = \frac{A}{T} \exp\left(-\frac{E_a}{kT}\right) \quad (4)$$

The activation energy (E_a) for hopping can be calculated from the slopes of the linear part of $\ln \sigma T$ versus $1000/T$ plots. The constant A involves the carrier concentration as well as other material-dependent parameters.[21] The E_a values as well as the temperature range at which they are valid are given in Table 3.

Attempt was also made to investigate the conductivity relaxation properties. At lower temperature range, if the chemical diffusion can be assumed to be the rate determining step, the following equation can be obtained under appropriate boundary conditions[22]:

$$\frac{\sigma(t)-\sigma(0)}{\sigma(\infty)-\sigma(0)} = 1 - \sum_{n=0}^{\infty} \frac{8}{(2n+1)^2\pi^2} \times \exp\left[-\frac{(2n+1)^2\pi^2 D_{chem} t}{4L^2}\right] \quad (5)$$

where in left part, $\sigma(0)$, $\sigma(t)$ and $\sigma(\infty)$ stand for the apparent conductivity at $t=0$ (initial), at t (during the relaxation process) and $t \to \infty$ (after reaching a time-independent equilibrium). In the right part, D_{chem} is the chemical diffusion coefficient, L the half of the sample thickness (diffusion length) and t is the time. Experimental and fitted data for $x=0.4$ sample are shown in Fig. 7. As expected, with the increasing of temperature, a rapid increase of relaxation rate was observed. The relaxation time for $T=400$ °C is about 30 times of that for $T=550$ °C, which can be illustrated by the change of chemical diffusion coefficient. The D_{chem} calculated was plotted in Fig. 8, the relation between D_{chem} and absolute temperature also satisfies the Arrhenius formula:

$$D_{chem} = D_0 \exp\left(-\frac{E_a}{kT}\right) \quad (6)$$

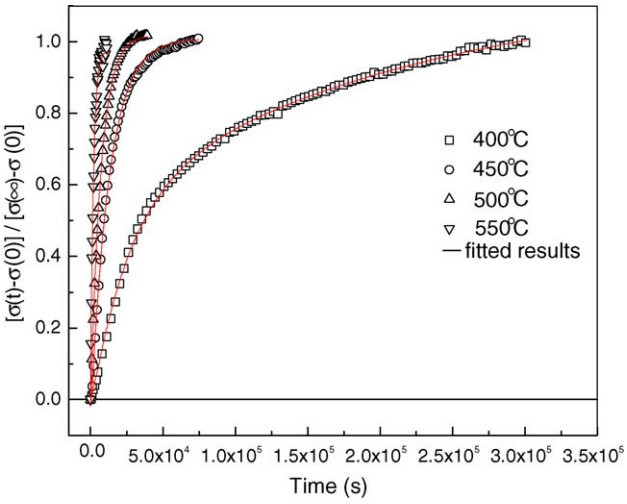

Fig. 7. Conductivity relaxation curves for $x=0.4$ sample measured at 400, 450, 500, and 550 °C.

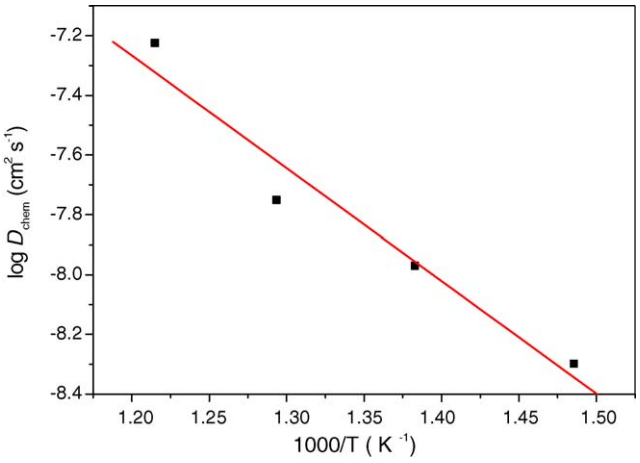

Fig. 8. Arrhenius plot of chemical diffusion coefficients.

where D_0 is the pre-exponential factor. The active energy (E_a) obtained is about 72.2 kJ mol^{-1}. At higher temperature ($T>550$ °C), the relaxation process is not obvious, which must be determined by sudden change of the oxygen partial pressure.[23,24]

4. Conclusions

Perovskite oxides of $Ba_xSr_{1-x}Co_{0.8}Fe_{0.2}O_{3-\delta}$ ($0.3 \le x \le 0.7$) were synthesized by the citrate-EDTA complexing method, which were identified as cubic structure for $x \le 0.6$ by XRD. And the lattice constant increased with the increase content of Ba doping. Generally, both the TEC values and electrical conductivity followed the opposite behavior. The formation of oxygen vacancies and the reduction of B-site cations play important roles in expansion and conduction properties at elevated temperatures. The average TEC values were larger than 20×10^{-6} °C^{-1} at measured range, and

the TEC values between 500 and 700 °C are extraordinarily high. The electrical conductivity were larger than 30 S cm^{-1} when $x \leq 0.5$ at above 500 °C. In a word, compositions with 40 and 50 mol% barium content are potential candidates for SOFC cathode application, whose electrochemical properties still need further investigations.

Acknowledgements

The authors gratefully acknowledge financial supports from the Ministry of Science and Technology of China under contrast no. 2001AA323090. The authors were also grateful to Weixiong Zhao (Anhui Institute of Optics and Fine Mechanics Chinese Academy of Sciences) for his friendly help.

References

1. Steel, B. C. H., Ceramic ion conducting membranes. *Curr. Opin. Solid State Mater. Sci*, 1996, **1**, 684–691.
2. Singhal, S. C., Advances in solid oxide fuel cell technology. *Solid State Ionics*, 2000, **135**, 305–313.
3. Stevenson, J. W., Armstrong, T. R., Carneim, R. D., Peederson, L. R. and Weber, W. J., Electrochemical properties of mixed conducting perovskites $La_{1-x}M_xCo_{1-y}Fe_yO_{3-\delta}$ (M = Sr, Ba, Ca). *J. Electrochem. Soc*, 1996, **143**, 2272–2279.
4. Shao, Z., Yang, W., Cong, Y., Dong, H., Tong, J. and Xiong, G., Investigation of the permeation behavior and stability of a $Ba_{0.5}Sr_{0.5}Co_{0.8}Fe_{0.2}O_{3-\delta}$ oxygen membrane. *J. Membr. Sci*, 2000, **172**, 177–188.
5. Fleig, J. and Maier, J., The polarization of mixed conducting SOFC cathodes: effects of surface reaction coefficient, ionic conductivity and geometry. *J. Eur. Ceram. Soc*, 2004, **24**, 1343–1347.
6. Teraoka, Y., Zhang, H. M., Furukawa, S. and Yamazoe, N., Oxygen permeation through perovskite-type oxides. *Chem. Lett.*, 1985, 1743–1746.
7. Huang, K., Wan, J. and Goodenough, J. B., Oxide-ion conducting ceramics for solid oxide fuel cells. *J. Mater. Sci*, 2001, **36**, 1093–1098.
8. Pei, S., Kleefisch, M. S., Kobylinski, T. P., Faber, J., Udovich, C. A., Zhang-McCoy, V. *et al.*, Failure mechanisms of ceramic membrane reactors in partial oxidation of methane to synthesis gas. *Catal. Lett.*, 1995, **30**, 201–212.
9. Shao, Z., Xiong, G., Tong, J., Dong, H. and Yang, W., Ba effect in doped $Sr(Co_{0.8}Fe_{0.2})O_{3-\delta}$ on the phase structure and oxygen permeation properties of the dense ceramic membranes. *Sep. Purif. Technol.*, 2001, **25**, 419–429.
10. Li, D., Liu, W., Zhang, H., Jiang, G. and Chen, C., Fabrication, microstructure, mechanical strength and oxygen permeation of Ba(Sr)Zr(CoFe)O_3-particles-dispersed $Ba_{0.5}Sr_{0.5}Co_{0.8}Fe_{0.2}O_{3-\delta}$ mixed-conducting composites. *Mater. Lett.*, 2004, **58**, 1561–1564.
11. van Veen, A. C., Rebeilleau, M., Farrusseng, D. and Mirodatos, C., Studies on the performance stability of mixed conducting BSCFO membranes in medium temperature oxygen permeation. *Chem. Commun.*, 2003, 32–33.
12. Shao, Z. and Haile, S. M., A high-performance cathode for the next generation of solid-oxide fuel cells. *Nature*, 2004, **431**, 170–173.
13. Shannon, R. D., Revised values of effective ionic-radii and systematic studies of interatomic distances in halides and chalcogenides. *Acta Cryst.*, 1976, **A32**, 751–753.
14. Teraoka, Y., Yoshimatsu, M., Yamazoe, N. and Seiyama, T., Oxygen-sorptive properties and defect structure of perovskite-type oxides. *Chem. Lett.*, 1984, 893–896.
15. Tai, L.-W., Nasrallash, M. M., Anderson, H. U., Sparlin, D. M. and Sehlin, S. R., Structure and electrical properties of $La_{1-x}Sr_xCo_{1-y}Fe_yO_3$. Part 1: The system $La_{0.8}Sr_{0.2}Co_{1-y}Fe_yO_3$. *Solid State Ionics*, 1995, **76**, 259–271.
16. Kostogloudis, G. Vh., Fertis, P. and Ftikos, Ch., The perovskite oxide system $Pr_{1-x}Sr_xCo_{1-y}Mn_yO_{3-\delta}$: crystal structure and thermal expansion. *J. Eur. Ceram. Soc.*, 1998, **18**, 2209–2215.
17. Shaula, A. L., Kharton, V. V., Vyshatko, N. P., Tsipis, E. V., Patrakeev, M. V., Marques, F. M. B. and Frade, J. R., Oxygen ionic transport in $SrFe_{1-y}Al_yO_{3-\delta}$ and $Sr_{1-x}Ca_xFe_{0.5}Al_{0.5}O_{3-\delta}$ ceramics. *J. Eur. Ceram. Soc.*, 2005, **25**, 489–499.
18. Uhlenbruck, S. and Tietz, F., High-temperature thermal expansion and conductivity of cobaltites: potentials for adaptation of the thermal expansion to the demands for solid oxide fuel cells. *Mater. Sci. Eng. B*, 2004, **107**, 277–282.
19. Petric, A., Huang, P. and Tietz, F., Evaluation of La—Sr—Co—Fe—O perovskites for solid oxide fuel cells and gas separation membranes. *Solid State Ionics*, 2000, **135**, 719–725.
20. Carter, S., Selcuk, A., Chater, R. J., Kajda, J., Kilner, J. A. and Steele, B. C. H., Oxygen transport in selected nonstoichiometric perovskite-structure oxides. *Solid State Ionics*, 1992, **53–56**, 597–605.
21. Minh, N., Ceramic fuel cells. *J. Am. Ceram. Soc.*, 1993, **76**, 563–588.
22. Mauvy, F., Bassat, J. M., Boehm, E., Dordor, P., Grenier, J. C. and Loup, J. P., Chemical oxygen diffusion coefficient measurement by conductivity relaxation-correlation between tracer diffusion coefficient and chemical diffusion coefficient. *J. Eur. Ceram. Soc.*, 2004, **24**, 1265–1269.
23. Bouwmeester, H. J. M., Den Otter, M. W. and Boukamp, B. A., Oxygen transport in $La_{0.6}Sr_{0.4}Co_{1-y}Fe_yO_{3-\delta}$. *J. Solid State Electrochem.*, 2004, **8**, 599–605.
24. Huang, K. and Goodenough, J. B., Oxygen permeation through cobalt-containing perovskites: surface oxygen exchange vs. lattice oxygen diffusion. *J. Electrochem. Soc.*, 2001, **148**, E203–E214.